



## Investigate the effects of urban land use on PM<sub>2.5</sub> concentration: An application of deep learning simulation

Liyuan Zhao <sup>a,\*</sup>, Ming Zhang <sup>b</sup>, Si Cheng <sup>c</sup>, Yunhao Fang <sup>a</sup>, Shuxian Wang <sup>a</sup>, Cong Zhou <sup>a</sup>

<sup>a</sup> School of Architecture and Urban Planning, Huazhong University of Science and Technology, Wuhan, China

<sup>b</sup> Community and Regional Planning Program, School of Architecture, University of Texas at Austin, Austin, USA

<sup>c</sup> Urban Planning & Design Institute of Shenzhen, China



### ARTICLE INFO

#### Keywords:

Land use  
PM<sub>2.5</sub>  
Density  
Deep learning

### ABSTRACT

As the fine particulate matter (PM<sub>2.5</sub>) polluting seriously threat people's health, exploring its mitigation strategies has become an urgent issue to be studied. Urban land use, the carrier of urban functions and human activities, has been widely recognized as an important contributor of PM<sub>2.5</sub> pollution. Taking Wuhan metropolitan area as an example, this study employs a deep learning simulation method to explore the effects of land use types and density on the spatial distribution of PM<sub>2.5</sub> pollutants. The PM<sub>2.5</sub> concentration data, raster-based land use data and meteorological conditions data are analyzed to identify their dynamic spatiotemporal characteristics. The meteorological conditions, including temperature and wind speed, are incorporated into the simulation platform, which improves the precision significantly. The simulation results show that PM<sub>2.5</sub> concentration caused by construction land such as industrial, residential, transportation, logistics and warehousing, commercial, utilities, and public service sequentially decreases. The impact of FAR on PM<sub>2.5</sub> concentration is spatially different. With the increase of FAR, some north construction pixels present PM<sub>2.5</sub> mitigation effects while a few grids in the south appear heavier pollution. By analyzing the results of different simulation scenarios, specific spatial-based PM<sub>2.5</sub> mitigation strategies and control measures are provided to promote healthy and sustainable urban development. This method can be transferred and applied to other metropolitans, so as to provide as a reference for policymakers and urban planners to promote effective air pollution mitigation strategies from the view of spatial planning.

### 1. Introduction

Many cities in the emerging economies are suffering from air quality deterioration associated with rapid industrialization and urbanization. One particular concern is urban exposure to the pollutant of the fine particulate matter (PM<sub>2.5</sub>) that poses severe threats to public health [1]. Mitigating PM<sub>2.5</sub> pollution has become a priority on the agenda of public agencies to improve the living environment. As the carrier of urban functions, urban land use plays a significant role in the spatial processes of PM<sub>2.5</sub> emission and diffusion [2]. Understanding the effects of urban land use on PM<sub>2.5</sub> concentration and dispersion is thus essential to formulating planning and policy strategies for mitigating PM<sub>2.5</sub> impacts on the urban living environment.

There have been voluminous studies on the differentiated effects of urban land uses contributing to PM<sub>2.5</sub> pollution [3,4]. Many studies examine the spatial correlation between PM<sub>2.5</sub> concentration patterns

and various types of land uses, including residential, industrial, transportation, green space, and others [4,5]. Studies have also found that PM<sub>2.5</sub> concentration varies by different urban form attributes such as density, compactness, and degree of centering [6,7]. In addition, traffic characteristics on various types of streets and highways explain PM<sub>2.5</sub> intensity along the roadway network [8]. Urban meteorological conditions also matter to PM<sub>2.5</sub> aggregation and diffusion [9,10]. While the existing studies have generated valuable empirical knowledge on the land use-PM<sub>2.5</sub> pollution relationship, much remains to be learned because of the dynamic and complex nature of PM<sub>2.5</sub> pollution. Recent advance in computing and data technologies offers a great potential to gain new insights into the effects of urban land use on PM<sub>2.5</sub> concentration and dispersion. A few studies have attempted to explore this potential [11–14]. This study contributes to the data technology-supported efforts by taking a deep learning simulation approach.

\* Corresponding author.

E-mail addresses: [liyuanzhao@hust.edu.cn](mailto:liyuanzhao@hust.edu.cn), [liyuanzhao2009@gmail.com](mailto:liyuanzhao2009@gmail.com) (L. Zhao).

## 2. Review of related studies

### 2.1. Impacts of land use on PM<sub>2.5</sub>

Traditional studies of urban land use impacts on PM<sub>2.5</sub> pollution focus on the mechanisms of the spatial distribution characteristics of residential, industrial, transportation, green space and other land uses on PM<sub>2.5</sub> concentration distribution. At present, there is a basic consensus that industrial and residential land exacerbate PM<sub>2.5</sub> concentration, while green area negatively associates with PM<sub>2.5</sub> concentrations [3,5]. Mao et al. (2012) found that land use/cover has a stable influence on PM<sub>2.5</sub> concentration, with a descending order of the impacts of different land types on PM<sub>2.5</sub> concentration: construction lands, open lands, water, farmlands, grasslands and woodlands [6]. Population density and characteristics of urban form such as degree of centering, and compactness also play significant impacts on PM<sub>2.5</sub> pollution [7,8]. Urban form at metropolitan and neighborhood scales affected PM<sub>2.5</sub> concentration in different ways [4,15]. Lu et al. (2020) found that in the East China Plain and Taklimakan desert; artificial surfaces, cultivated land and deserts were coated with high PM<sub>2.5</sub> concentration more frequently, while the forest, grassland and unused land were usually covered with low PM<sub>2.5</sub> concentration [2].

A number of traffic and built environmental factors were identified as important predictors of near road ultrafine particles, that industrial zoning, main roads and highways exacerbates PM<sub>2.5</sub> pollution [5,9]. Rail transit can reduce PM<sub>2.5</sub> pollution and have a significant effect on improving air quality in the long run, while its construction has a negative short-term effect [16]. Zhao et al. (2021) investigated the coupling effect of urban lake wetlands and the neighboring greenery on air PM<sub>10</sub> and PM<sub>2.5</sub> levels in Wuhan, China, and demonstrated that combination of lakes and greenery can support a reduction in PM concentrations in the neighboring area [17].

Overall, the association of land use elements with PM<sub>2.5</sub> has been investigated extensively. Nevertheless, most previous studies have examined this relationship using remote sensing satellite data and traditional statistical method, which ignore the compound effects of detailed urban construction land types and intensity on PM<sub>2.5</sub> concentrations. The correlation analysis under multiple scenarios using recent advanced deep learning simulation approach is beneficial for researchers to achieve a deeper understanding of the effects of urban land use on PM<sub>2.5</sub> concentration.

### 2.2. Meteorological conditions and PM<sub>2.5</sub> concentrations

Existing studies on the relationship between urban land use and PM<sub>2.5</sub> have significant differences. As an example, the results of the effect of residential land use on PM<sub>2.5</sub> pollution, some studies point to a positive exacerbating effect [3], while others conclude a negative correlation [5,16]. The reason is the complexity of PM<sub>2.5</sub> influencing factors. These studies tend to ignore the effect of urban meteorological conditions on the clustering and dispersion of PM<sub>2.5</sub> pollution, which may also be one of the reasons for the variability of the findings.

Many studies show that PM<sub>2.5</sub> pollution is closely related to urban meteorological conditions, which affect the aggregation and diffusion of PM<sub>2.5</sub> through factors including relative humidity, precipitation, temperature and wind speed [10,11,18,19]. Guo et al. (2022) investigated relationships between different levels of air pollution with meteorological parameters including wind speed, temperature inversion and weather type [20]. Duan et al. (2021) showed that temperature always had a positive influence on PM<sub>2.5</sub> and wind speed had a varied impact on PM<sub>2.5</sub> within the high-density city, Shenzhen [21]. Chen et al. (2018) indicated that meteorological influences on PM<sub>2.5</sub> concentrations have notable seasonal and regional variations, and factors including temperature, humidity and wind, play much larger effect at the national scale [22]. By using a complex coupling pattern, Zou et al. (2021) proved that PM<sub>2.5</sub> pollution changes with seasons and relative humidity

is a consistent driving factor [23]. Li et al. (2021) found that atmospheric pressure are the key factors contributing to the temporal and spatial variation of PM<sub>2.5</sub> pollution in Zhejiang, China [24]. However, existing research of impact of land use on PM<sub>2.5</sub> often lacks meteorological data and ignores the influence of urban meteorological conditions on PM<sub>2.5</sub> aggregation and diffusion. Therefore, the integration of high-precision meteorological data is of great significance to improve the reliability of research results.

### 2.3. Deep learning and its application

Existing studies mainly uses empirical statistical methods and land use regression (LUR) model and Geographically weighted regression (GWR) model to explore the relationship between land use and air quality [25]. Unfortunately, empirical statistical methods, such as correlation analysis [26,27] and linear regression method [28–30] usually take the group mean across a city as statistical samples, ignoring the spatial formation mechanisms of air pollution, which could lead to lack of precision [31]. LUR model has become a popular approach to explore spatial and temporal variations of PM<sub>2.5</sub> concentration [11]. However, it is difficult for LUR models to integrate complicated related spatial-temporal factors of the aggregation and diffusion of PM<sub>2.5</sub> concentration [32]. GWR model can effectively link geographical locations and take spatial-temporal changes into account, which enable it to explore the spatial heterogeneity of PM<sub>2.5</sub> and its influencing factors [33,34]. But there is considerable uncertainty in the process of GWR [35].

Along with the booming development of computer science and information technology, artificial intelligence and machine learning has become a popular method. Deep learning, as a novel machine learning method with fast training and high accuracy, has gained popularity over the past few years. It has been successfully applied to face intelligent recognition, remote sensing imaging classification, medical computer-aided diagnosis and other fields [36–39].

The convolutional neural networks (CNNs) in deep learning can process either two- or three-dimensional images ingested in their input layer, thus enabling them to learn from urban maps in urban planning, such as land use map, air quality data and meteorological images [40, 41]. Previous studies have successfully applied deep learning in many fields of urban planning, such as urban spaces reclassification [42–44], land use change and land cover simulation [45], traffic demand prediction and transportation safety planning [46,47], and urban environmental solution [48,49], which proves its advantages of accurate, reliable and intelligent method for urban research.

Among different deep learning methods, the convolutional neural networks have high efficiency of performance because of a hierarchical structure of learning layers [46]. Compared with traditional mathematical statistics methods, CNNs are flexible for high-dimensional data because of its characteristics of sharing convolution kernel parameters. Remote sensing images, land use spatial data, mobile devices data, and other disaggregate data can all be used as the input data [50]. It also allows the use of a high spatial-resolution data to determine the effects of land use and its neighborhood factors at specific geospatial locations, achieving a higher prediction accuracy [46,51]. It does not need to extract features manually and the features can be automatically derived through model training process. In addition, by performing visual simulations of predictive results under different scenarios, CNNs allow to make better precise location-based predictions and provide corresponding adaptation regarded to specific geospatial locations [50].

Recently, some studies have adopted deep learning methods to explore the impact of urban land use on PM<sub>2.5</sub> concentration. For example, Chen et al. (2021) used random forests model to estimate PM<sub>2.5</sub> concentrations through remote sensing, meteorological and land use information [12]. Wong et al. (2021) proposed a machine learning with LUR model to assess and predict the spatial-temporal variability of PM<sub>2.5</sub> [13]. However, these researches focus on the effects of urban built

area, forest, green land, green land and water area. Better land use data could help to build a better model to generate land use allocations strategies for people to inhabit [13]. The detailed classifications of construction lands in urban area such as residential, industrial, commercial and services, institutional lands are rarely considered. These various artificial surfaces and their spatial layout are closely associated with PM<sub>2.5</sub> concentration which are critical to the optimizing air quality oriented urban spatial planning [2,52]. Therefore, the employment of CNNs to explore the relationship between detailed construction land and PM<sub>2.5</sub> concentration is promising in providing intuitive and scientific guidance for sustainable development and urban pollution control.

### 3. Method

#### 3.1. Study area and data

Wuhan, located in central China, is concentrated of heavy industries and manufacturing industries, with rainy summers, cold and wet winters, and serious air pollution. Currently, many studies focuses on air pollution in Wuhan at inner urban area or neighborhood scale [53,54]. There small-scale studies emphasize internal spontaneous forms of pollution and ignore the role of external space [55]. However, local urban air pollution is often caused by excessive air pollution in surrounding areas due to its characteristics of externality [56]. To better capture the externality of air pollution, the Wuhan metropolitan area is selected as the research region, which covers an area of 3261 km<sup>2</sup>, including urban area with the size of 872 km<sup>2</sup> and remaining 2434 km<sup>2</sup> suburban area (Fig. 1).

The initial data includes air quality monitoring station data and PM<sub>2.5</sub> concentration data provided by the Wuhan Environmental Protection Bureau, land use data of Wuhan metropolitan area provided by the Wuhan Nature Resource and Planning Bureau, and meteorological data provided by the China Meteorological Administration. There are meteorological monitoring stations in the study area, and the meteorological indicators such as yearly average temperature and wind speed are used. Based on the mentioned above initial data, the attributes including PM<sub>2.5</sub> concentration, land use type, land use intensity, elevation, temperature and wind speed were read and processed using ArcGIS and MATLAB software to prepare for deep learning simulation model.

The original PM<sub>2.5</sub> concentration data obtained from the monitoring stations is point data, but the simulation model requires polygon data that covers whole Wuhan metropolitan area. Kriging interpolation was employed to predict the PM<sub>2.5</sub> concentration and meteorological value of new data points based on observed value from existing monitoring

stations. By calculating weighted averages from the neighboring data, Kriging interpolation can capture data outside the monitoring site [57, 58], and has been demonstrated as an effective estimation method of predicting spatial distribution of PM<sub>2.5</sub> and meteorological conditions across the region [14,25]. These data were then converted into 10 m × 10 m raster data (Fig. 2).

Because of the large area of the Wuhan metropolitan area, each independent variable data contains a data matrix with size of 6997 × 6767, which may cause memory overflow if directly input into the model for training. Therefore, sample data sets with smaller matrices at the same size need to be selected and input into the model for training in batches. The wind speed, average temperature, existing land use and classified PM<sub>2.5</sub> raster data of Wuhan metropolitan area in 2016 were cropped into 2650 small raster samples of 128 × 128 (an area of 1280 m × 1280 m) using ArcGIS software. Due to the irregular shape of study area, the square matrix along the range boundary has no data and needs to be removed, and finally there are 1835 small raster samples.

#### 3.2. Model framework

This study builds a deep learning-based simulation model to analyze and visualize the spatial distribution of PM<sub>2.5</sub> under different land use development scenarios. Fig. 3 illustrates the modeling framework: model construction, model training, and scenario analysis. First, the study constructs an Unet CNN model that integrates network architecture layers, input layer and output layer. The input layer includes land use (type and intensity), elevation and meteorological maps (temperature and wind speed), whereas the output layer illustrates PM<sub>2.5</sub> concentration. Second, the constructed model is trained to achieve a desired level of model reliability and stability. Training is crucial step since it identifies the dynamic linkage between the input and output layers and often involves nonlinear activation functions [59]. The third part of the model applies the trained model to simulate future PM<sub>2.5</sub> spatial distribution in different scenarios of land use types and intensity. By comparing the simulated results of different scenarios, sensitive and heavily polluted land pixels can be identified, which helps to reveal the relationship between land use factors and PM<sub>2.5</sub> distribution patterns.

#### 3.3. Unet CNN model

Built upon the UNet architecture, a deep convolutional neural network is constructed to explore the impacts of land use related spatial attributes on the PM<sub>2.5</sub> concentrations. UNet neural network architecture was first applied to semantic segmentation of medical images with limited amounts of data. It contains contraction path in the left half and

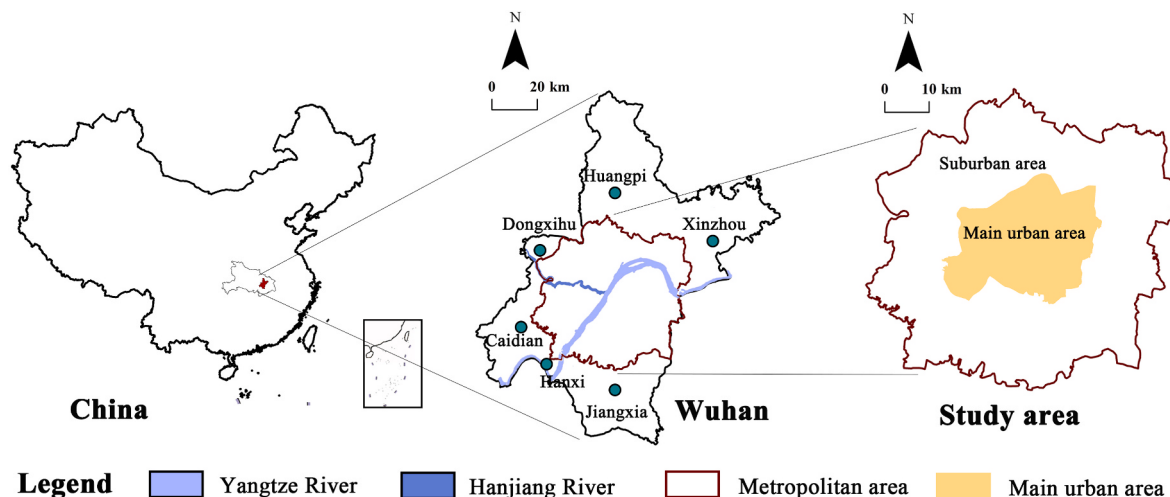


**Fig. 1.** Description of Wuhan metropolitan area.

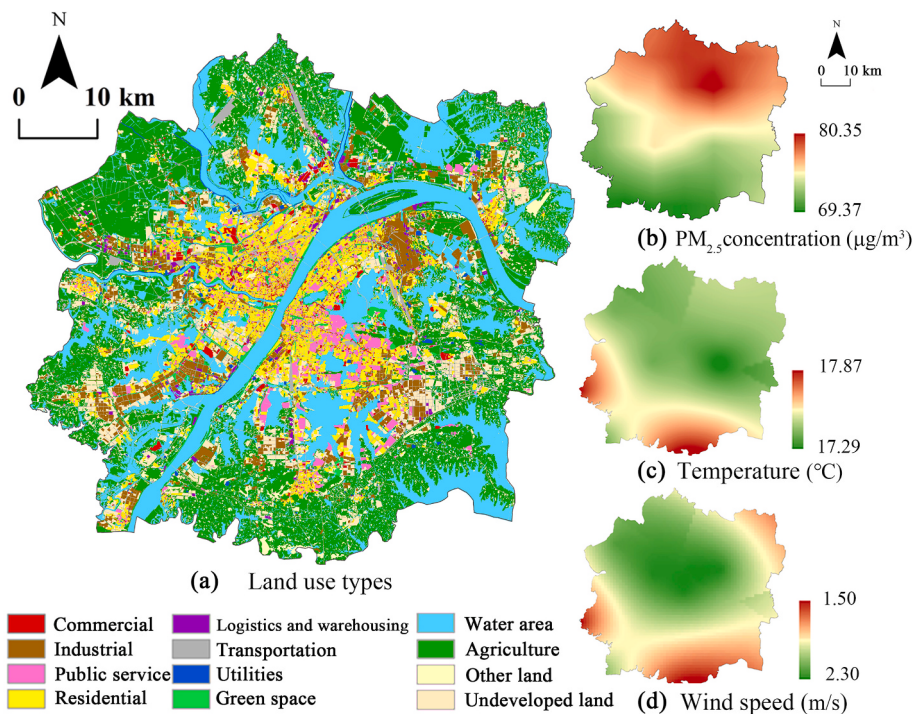


Fig. 2. Spatial distribution of related factors in: (a) Land use types; (b)  $\text{PM}_{2.5}$  concentration; (c) Temperature; (d) Wind speed.

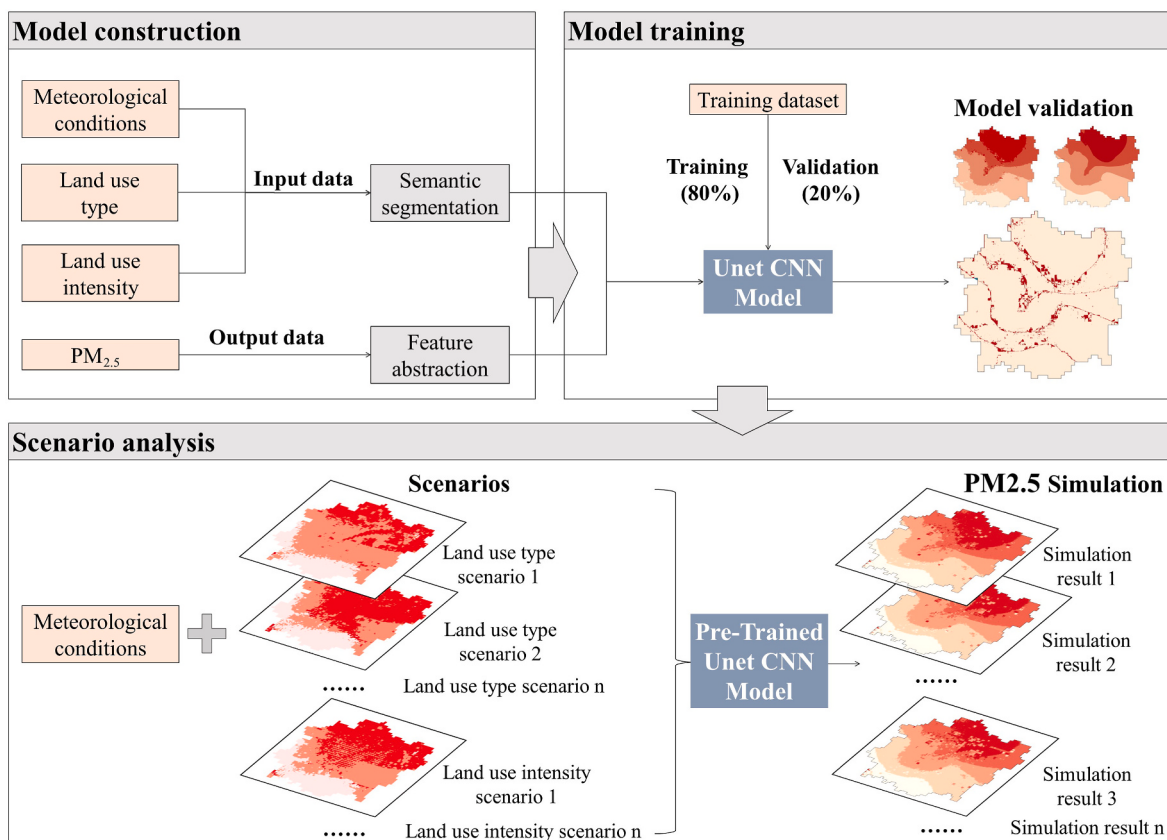
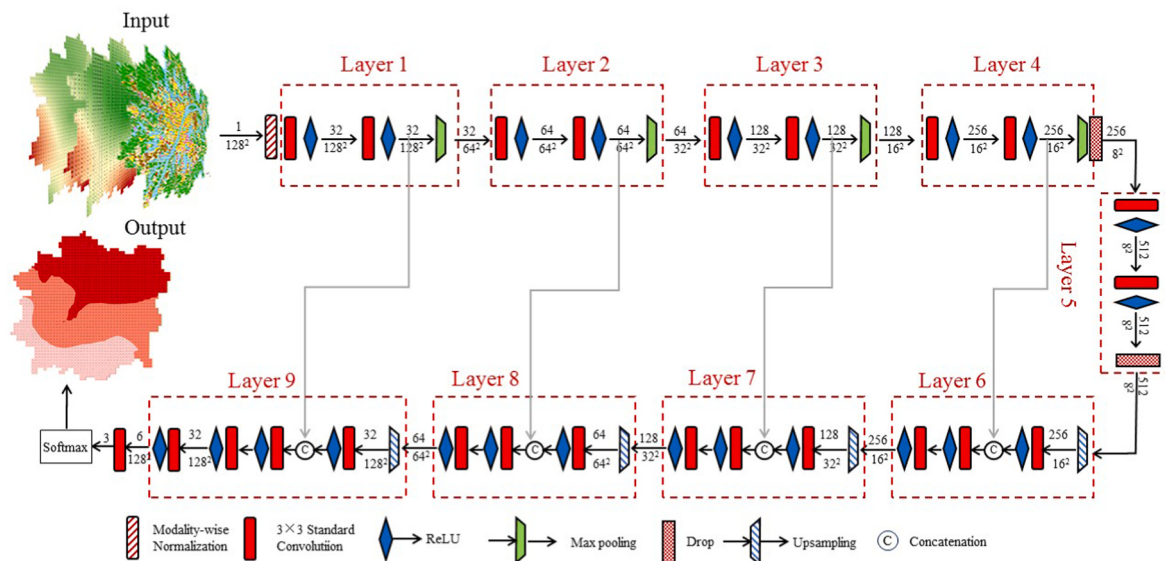


Fig. 3. Model framework for deep learning-based simulation model.

expanding path in the right half, so named because of the U-shaped structure. The contraction path, namely as encoder, aims to capture and extract the image feature automatically. The expanding path, called as

decoder, is responsible for upsampling and localizing features into specific locations with high resolution. Fig. 4 illustrates the structure of a UNet semantic segmentation model.



**Fig. 4.** Schematic diagram of the structure of UNet semantic segmentation model.

UNet is an end-to-end fully convolutional network. In our developed UNet model, the contraction path is a typical fully convolutional neural network (CNN), including two  $3 \times 3$  convolution layers, each followed by a rectified linear unit (ReLU) and one  $2 \times 2$  pooling operation with stride 2 for down-sampling. At each down-sampling step, the number of feature channels are doubled. By repeatedly implementing these convolutions and polling operations, the feature of the input land use related factors affecting the spatial distribution of PM<sub>2.5</sub> concentration can be effectively captured and extracted.

The expanding path is composed of four parts. First, the size of the image is doubled through deconvolution, and the number of feature channels is halved. These deconvolved features are then concatenated with the correspondingly cropped feature maps from the contracting path on the left to form an image of doubled size. Finally, two more  $3 \times 3$  convolutions and each followed by a ReLU are performed to extract more features related to PM<sub>2.5</sub> concentration changes. These two convolutions enable to extract more image features and recover the pixel size so that the extracted information can be precisely located to the specific spatial location of the input image. Specifically, as shown in Fig. 4, the input images are land use and meteorological condition data, and the output is PM<sub>2.5</sub> concentration, with the size of 128×128. Through four down-sampling of the upper contraction channel, a number of 256 pieces 8×8 images are generated. In the lower expansion channel, after deconvolution, concatenation, and two convolutions process, the images are then restored as the size of 128×128 images, so as to complete the image feature extraction and enable precise localization. The output of the model, is a pixel-by-pixel mask, that shows the predicted class of PM<sub>2.5</sub> concentration for each pixel. UNet architecture proved itself very useful for segmentation problems, that yields precise segmentations with very few training images [38].

### (1) Convolutional layer

As the most important hidden layer of the CNN, convolutional layer aims to create feature maps from input images. It first convolves image features with a certain number of convolution kernels to create different feature images. These feature images are then combined to generate a new output of convolution layer. Deeper layers can better capture global information with large spatial extent [60]. The number of output feature images is the same as the number of convolution kernels. In this study, the relationship between the feature images of land status, average temperature and wind speed, with the spatial distribution of PM<sub>2.5</sub>

concentration is modeled by the convolution operation. The  $j$ th feature map in layer  $l+1$ , denoted by  $x_j^{(l+1)}$  can be formulated as:

$$x_j^{(l+1)} = f \left( b_j^{l+1} + \sum_{j \in M_i^l} x_i^l * w_{ij}^{l+1} \right) \quad (1)$$

where  $x_j^{l+1}$  is the output value of unit  $j$  in layer  $l$ ,  $f$  is the activation function;  $x_i^l$  is the input feature of unit  $j$  in layer  $l$ ,  $w_{ij}^{l+1}$  is the weight parameter between unit  $i$  in layer  $l$  and unit  $j$  in layer  $l+1$ , and  $b_j^{l+1}$  is the bias parameter of unit  $j$  in layer  $l+1$ .  $M_i^l$  means the total number of feature maps from previous layer  $l$ , and equals the number of convolution kernels.

Set the padding as  $p$ , the sliding step of the convolution kernel, namely, stride as  $s$ , after the convolution operation, the size of the output feature maps of layer  $l+1$  can be denoted as:

$$n_1^{(l+1)} = (n_1^l + 2p - h^{(l)}) / s + 1 \quad (2)$$

$$n_2^{(l+1)} = (n_2^l + 2p - h^{(l)}) / s + 1 \quad (3)$$

### (2) Activation function

Activation functions (AFs) are then applied to every neuron in the convolutional layers, so they highly influence the output of CNNs [40]. Their performances are critical to the accuracy and reliability of CNNs. AFs enable the network with the capability of simulating nonlinear functions. AFs perform nonlinear transformations within the convolutional layers, which provide the layers of CNNs with the gradient required to learn from non-linear data. In this study, Rectified Linear Unit (ReLU) is introduced in our proposed CNNs due to its advantages of solving vanishing gradients problems, high computational power and fast convergence [61], which can be defined as  $f(x) = \max(0, x)$ .

### (3) Pooling layer

Multiple convolutional layers will increase the number of feature maps, resulting in high computational burdens. Pooling layer is a kind of down-sampling layer designed to compress the key factors that affect the spatial distribution of PM<sub>2.5</sub> concentration extracted after convolution,

thereby improving the computational efficiency of the whole network. Specifically, there are two typical pooling operations: average and maximum, which windows are placed at non-overlapping positions  $D$  in each feature map and the average or maximum values of each window are maintained. The two operations can be described as:

$$\bar{x} = \frac{1}{M} \sum_{(i,j) \in D} x_{ij} \quad (4)$$

$$x_{max} = \max_{(i,j) \in D} x_{ij} \quad (5)$$

where  $M$  denotes the total number of windows, and  $x_{ij}$  is the value of each pixel. Suppose the size of the kernel windows of pooling operation in pooling layer  $q$  is  $k \times k$ , the stride is  $s$ , and the size of input feature maps is  $m_1^{q-1} \times m_2^{q-1}$ , then the size of the output feature map obtained from the pooling layer  $q$  can be denoted as:

$$m_1^{(q)} = \left( m_1^{(q-1)} - k \right) / s + 1 \quad (6)$$

$$m_2^{(q)} = \left( m_2^{(q-1)} - k \right) / s + 1 \quad (7)$$

Existing researches have demonstrated the max pooling function is effective in dimension reduction, and capable of better preserve features [62]. Hence the max pooling function is employed in our CNN model.

#### (4) Dropout layer

Dropout layer is considered an approach that allows convolutional neural networks to work in practice, due to the efficiency of preventing overfitting and low computational requirements [63]. It reduces the interdependence of neurons or overdependence of certain neurons by randomly removing some neurons and forcing them to combine into subnetworks for training. Each layer of the Dropout neural network has some unconnected neurons, and during the network training process, the parameters of the unconnected neurons will not be updated, while the remaining neurons constitute sub-network for training. In this way, different sub-networks are formed through multiple training sessions and ultimately combined into a complete neural network.

## 4. Results

### 4.1. Results of model training

In order to implement the Unet CNN model, a simulation platform based on several packages was constructed using Python 3.10. For clearly capturing the impact of urban land use factors on PM<sub>2.5</sub> concentration distribution, geographical elevation and meteorological conditions are also considered in the model. The output is the classification result of predicted PM<sub>2.5</sub> concentration. A total of 17 features of Wuhan metropolitan area in 2016 are selected as input variables, including 13 land use type attributes, 1 land use density factor, 1 elevation data and 2 meteorological features. In order to make better use of the Unet model to conduct migration learning on input data, this study uses One-Hot coding to store independent features for each land use type, and converts them into 13 features respectively representing a single land type. Specifically, the land use type inputs include, residential, commercial, industrial, public services, logistics and warehousing, transportation, utilities, green space, water area, agriculture, specially-designated land, rural land, and undeveloped area. There are a total of 1835 sample sets for each input variable. To ensure model simulation is valid, the variance inflation factor (VIF) is used for multicollinearity diagnostics of the inputs. The results show that the all the VIF values are less than 5, which means there is no c multicollinearity problem among inputs. The semantic segmentation simulation model randomly selected 80% of the samples for training, while the remaining 20% of the samples were used for validation.

The hyperparameters, including optimizer, activation function, learning rate, and the number of epochs, etc., are crucial in the training process of the Unet CNN model. To consolidate the UNet model with better fitness, hyperparameters are manually modified based on an iterative process until the model accuracy cannot be improved, as shown in Table 1. Choosing adaptive moment estimation (ADAM) as the optimizer can demonstrate better performance under sparse gradients. The activation function ReLU can reduce the vanishing gradient and has better convergence performance. We use the ReduceLROnPlateau callback function to reduce the learning rate to 0.00001 for enhancing model's performance [64]. After the model is successfully trained, the testing dataset is used to obtain the predicted values of the sample sequences. Then, all predicted subsequences are aggregated for final prediction.

### 4.2. Results of model validation

Validation is an important process for checking the effectiveness of the proposed deep learning model in capturing the relationship between input variables with PM<sub>2.5</sub>. Confusion matrix and kappa coefficients are used to compare the predicted and existing data [65–67]. The point-by-point accuracy for the training sample set, i.e. Kappa coefficient, is 96.9%, and for the test sample set is 81.8, achieving an acceptable prediction accuracy [68–70]. To verify the predictive performance, the entire sample dataset of independent variables is input into the model to predict PM<sub>2.5</sub> concentration. It achieves a high accuracy, 96.2%. The predicted PM<sub>2.5</sub> concentration map is shown in Fig. 5. Spatially, the predicted results are basically similar to the actual PM<sub>2.5</sub> concentration map. It proves the model's applicability in reflecting the relationship between land use attributes and PM<sub>2.5</sub> pollution.

### 4.3. Effects of land use type on the spatial distribution of PM<sub>2.5</sub>

To investigate the contribution of construction land types to PM<sub>2.5</sub> concentration distribution, a total of eight land use type scenarios are developed, namely: commercial scenario, industrial scenario, public service scenario, residential scenario, logistics scenario, transportation scenario, utilities scenario and green space scenario. In each scenario, a new map feature is generated by setting all its land pixels as its scenario's land type. For example, in the residential scenario, all pixels are converted into residential land. This new map feature is input into the trained model instead of previous residential map. In this way, a set of eight new map features are separately generated and input into the trained model. By comparing the model outputs of spatial distribution of PM<sub>2.5</sub> concentration under these scenarios, the impact of land type is explored and discussed.

As shown in Fig. 6, the predicted output of PM<sub>2.5</sub> concentration indicates that the pollution level in the south is roughly the same, but varies widely in the central and northern regions. Comparing the high PM<sub>2.5</sub> concentration values in each scenario, the heavy PM<sub>2.5</sub> pollution pixels in industrial (Fig. 6d), residential (Fig. 6a), transportation (Fig. 6f), and logistics and warehousing (Fig. 6e) scenarios are significantly higher than those in other scenarios. The results of green space scenario (Fig. 6h) are significantly lower. This indicates the development of industrial, residential, transportation, and warehousing will lead to heavier PM<sub>2.5</sub> pollution, while green space significantly reduces

**Table 1**  
Hyperparameter setting for UNet model.

Hyperparameters	Description	Hyperparameters	Description
Optimizer	Adam	Learning rate	0.00001
Activation function	ReLU	Min learning rate	0.0000001
Stride	1	Padding	Same
Kernel	32	Batch_size	4
Filter	3 × 3	Number of epochs	120

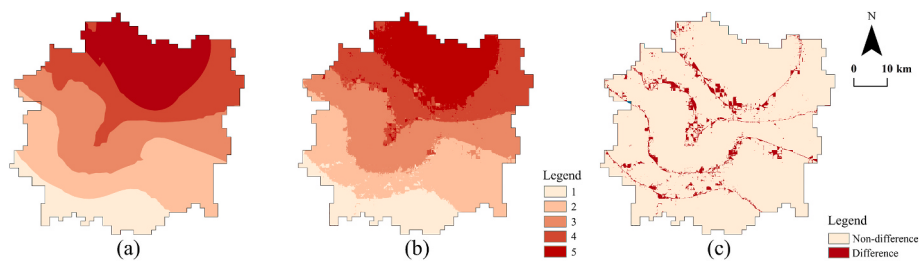


**Fig. 5.** PM<sub>2.5</sub> concentration in model validation: (a) Actual PM<sub>2.5</sub>; (b) Predicted PM<sub>2.5</sub>; (c) Spatial differences between actual and predicted PM<sub>2.5</sub>.

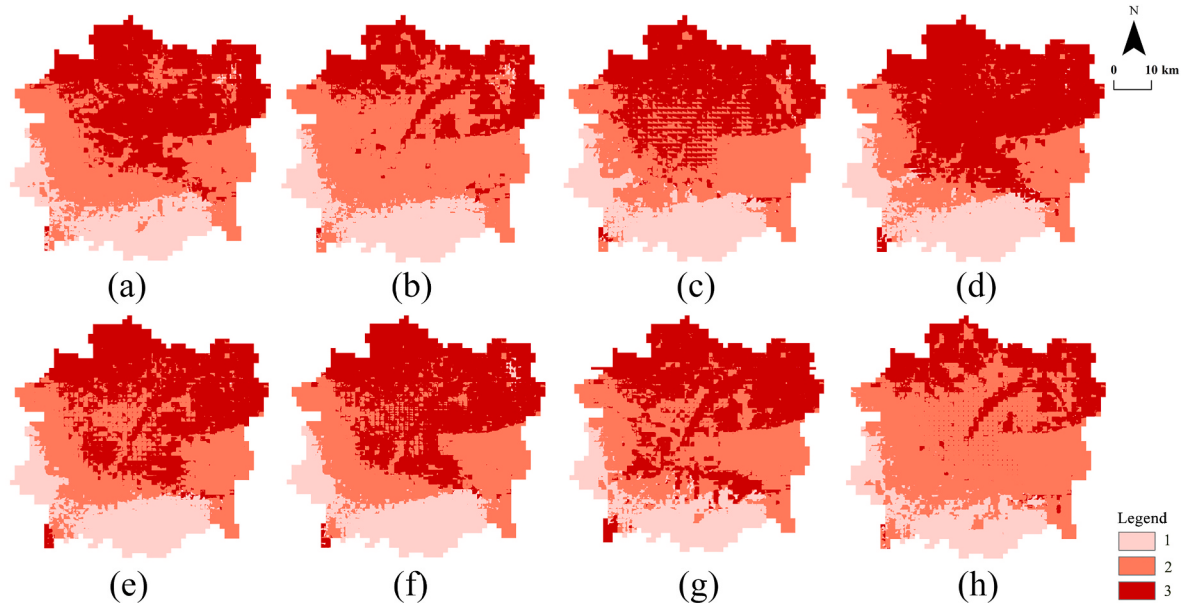


**Fig. 6.** PM<sub>2.5</sub> predicted results under land use type scenarios: (a) residential; (b) public service; (c) commercial; (d) industrial; (e) logistics and warehousing; (f) transportation; (g) utilities; (h) green space. (For interpretation of the references to colour in this figure legend, the reader is referred to the Web version of this article.)

PM<sub>2.5</sub> concentration. The PM<sub>2.5</sub> pollution caused by these land use types ranks in a descending order: industrial, residential, transportation, logistics and warehousing, commercial, utilities, public service, and green space.

The spatial aggregation and dissipation of PM<sub>2.5</sub> pollutants are closely related to the nature characteristics of land use environment. Some PM<sub>2.5</sub> pollutants are generated by activities carried on the construction land itself. Industrial land is most likely to cause high PM<sub>2.5</sub> pollution, as most production generates emissions of pollutants. Residential land is always accompanied by population concentration, and the high and dense buildings makes it not conducive to the diffusion of PM<sub>2.5</sub> pollutants. Transportation, logistics and warehousing lands generate vehicle emissions, leading to an intensification of PM<sub>2.5</sub> pollution. Green space, benefit from green plants, which have better sedimentation, flocculation, adsorption and inhalation effects on PM<sub>2.5</sub> pollutants, thereby effectively reducing pollution [5].

#### 4.4. Effects of land use intensity on the spatial distribution of PM<sub>2.5</sub>

This section explores the impact of land use intensity, measured by floor area ratio (FAR), on PM<sub>2.5</sub> concentration. The FAR of a specific plot refers to the ratio of the total building area to the plot area. It is a dimensionless ratio usually determined by the height of building. FAR is usually closely related to the area of buildings and population density. It has been proven as an important factor causing varying degrees of building occlusion, thereby altering the local air flow and affecting the

diffusion of PM<sub>2.5</sub> particles [71–74]. Three FAR scenarios are considered, shown as in Fig. 7. For each scenario, the FAR values increase by 0.5 (SFAR1), 1.0 (SFAR2) and 1.5 (SFAR3) respectively. Similar to scenarios of land use type, the new FAR map in each scenario is input to the trained model instead of original FAR input.

By analyzing the model results of three FAR scenarios, the impact of FAR is explored, shown as in Fig. 8. The changes in PM<sub>2.5</sub> caused by increasing FAR in SFAR3 are visualized in Fig. 9a. The PM<sub>2.5</sub> concentration level has been reclassified into levels 1–5 from low to high pollution. The effect of FAR on PM<sub>2.5</sub> concentration varies spatially. As FAR increases, some northern construction pixels (red pixels in Fig. 9a) show a mitigating effect while a few grids appear heavier pollution (green pixels in Fig. 9b). Specifically, under the third scenario (SFAR3), the simulated PM<sub>2.5</sub> pollution in the northern region shows lower level of PM<sub>2.5</sub> concentration. High FAR increases the windward side of the buildings, affecting internal air flow, which to some extent helps to resist the invasion of external pollutants and makes it difficult for inside pollutants to spread out [72]. Similar conclusions can also be found in recent research. Dense land urbanization results in a decrease in the PM<sub>2.5</sub> concentration in most urban areas for the same emission source [75]. In addition, according to the pollution source identification reports of Wuhan City, the external source of pollutants mainly invades from the north. Thus, increasing FAR in the north area can effectively resist the invasion of external pollutants. Dual effects alleviate the pollution in the northern region. However, some grids scattered in the south show serious pollution, which requires checking their local micro

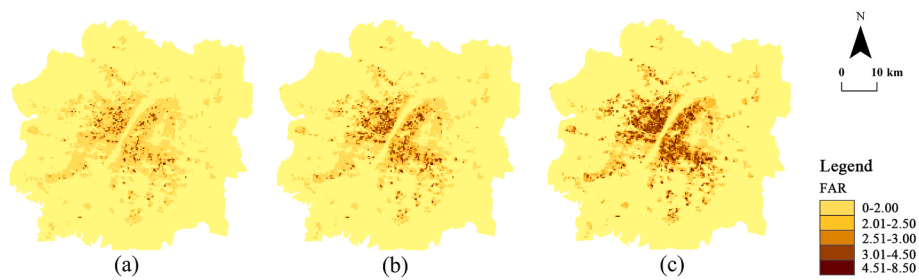


**Fig. 7.** FAR of construction land under three Scenarios: (a) SFAR1 (b)SFAR2 (c)SFAR3.

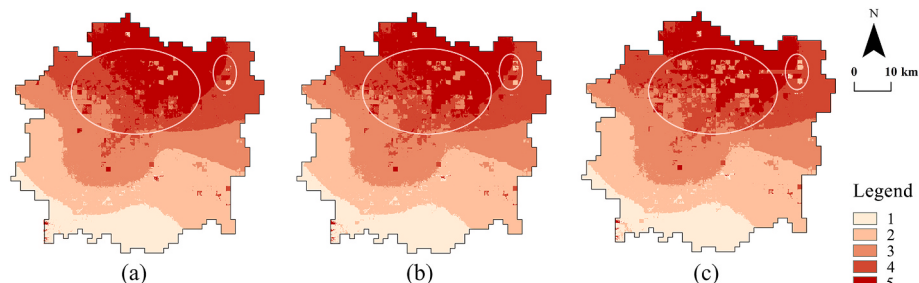


**Fig. 8.** Model results of PM<sub>2.5</sub> concentration (a) SFAR1 (b)SFAR2 (c)SFAR3.

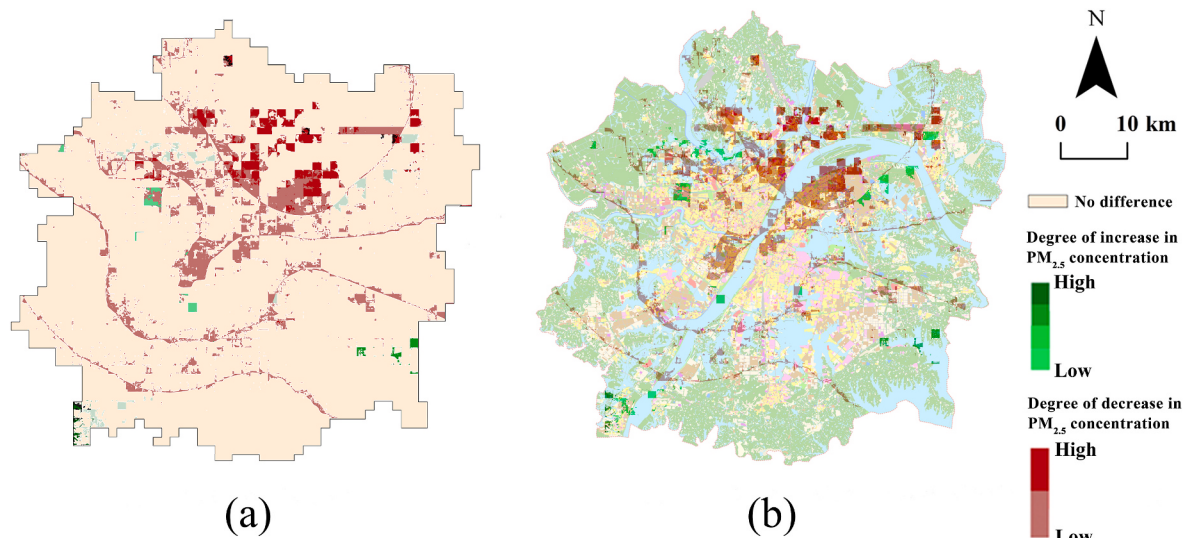


**Fig. 9.** Analysis of predicted PM<sub>2.5</sub> in SFAR3: (a) The changes of PM<sub>2.5</sub>; (b) The overlap of land use map and PM<sub>2.5</sub> in SFAR3.

characteristics.

With this question, the outputs of the third FAR scenario are compared with the baseline scenario and overlapped with the actual land use map, shown as Fig. 9b. The changes in PM<sub>2.5</sub> concentration from baseline to the SFAR3 scenario show that most PM<sub>2.5</sub> mitigated pixels are locate around water and forest land. The dust retention function of forest land enables it to reduce the concentration of particulate matter. Water bodies, as an important component of urban ventilation, also plays a positive impact on PM<sub>2.5</sub> diffusion. Combining previous results that high buildings help resist the invasion of pollutants, it further demonstrates that increasing FAR can largely mitigate the PM<sub>2.5</sub> concentration around water and forest area. Some grids surrounding express roads and industrial land have high PM<sub>2.5</sub> concentration. Increasing FAR around roads and industrial land hinders the evacuation of car exhaust and industrial emissions, which induces aggravated pollution. Basically, due to the difficulty of pollutants

diffusing from the pixels with high plot ratio to low plot ratio pixels, increasing FAR usually results in mitigation in low density area, but some special locations with self-generated pollution present heavier situation.

## 5. Land use planning and policy implications

### 5.1. Land use type spatial layout optimization strategy

Based on the effects of land use types on PM<sub>2.5</sub> pollution in Section 4.3, targeted optimization strategies are proposed to alleviate PM<sub>2.5</sub> pollution. The results in Section 4.3 indicate that industrial land is the main source of pollutants. Urban road transportation generates vehicle emissions, which are usually the component of ventilation corridors and play an important role in dissipation of pollution and improving the urban atmospheric environment. In this section, several typical

locations of industrial land and road transportation are selected to explore the optimization strategies according to the simulation results.

First, the most severe polluted industrial zones are selected. According to the data provided by Wuhan Planning and Design institute, there are ventilation corridors in Wuhan metropolitan area, as shown in Fig. 10. The Zhuankou industrial zone is centered in the upwind direction of Houguan lake ventilation corridor. Industrial enterprise Wuhan iron and steel company (WISCO), is located in the central part of East Lake ventilation corridor, which also aggravates the pollution in downwind area. In particular, the most severe polluted area lies to the north junction of Great East Lake ventilation corridor and Yangtze River ventilation corridor, including WISCO, Wuhu and Chenjiaji zones. These three industrial zones are taken as optimizing targets.

Then, the strategies for alleviating PM<sub>2.5</sub> for three industrial zones are proposed respectively, according to their location, surrounding land use and model results. The Wuhu area, as a large-scale residential land in the north, should improve green land and open space to enhance the abatement and diffusion capacity of PM<sub>2.5</sub>. From the long-term perspective, the heavily polluting enterprises, WISCO should be replaced by other urban function such as Industrial heritage. The Chenjiaji zone, composed of residential and industrial with well-developed surrounding water system, should increase recreation areas utilizing existing water body to reduce PM<sub>2.5</sub> pollution.

As for urban road traffic emissions, several mitigation strategies can be adopted, such as reducing long-distance commuting trips, increasing road network density, strengthening micro-circulation of branch roads, and increasing the proportion of new energy vehicles. Meanwhile, arterial road that is aligned with the direction with the wind corridors should be densified to enhance the diffusion capacity of PM<sub>2.5</sub> pollution. In addition, greening should be synergistically combined with the configuration both sides of the road network, because of its sedimentation, blocking, adsorption, and inhalation effects on PM<sub>2.5</sub> pollution.

## 5.2. FAR based land use spatial layout optimization strategy

The increase in FAR effectively alleviates the PM<sub>2.5</sub> pollution in most north pixels covered by abandon water and forest land. However, a small number of grids experience heavier pollution, located near concentrated industrial and residential land on the edge of the main urban area (green pixels in Fig. 9a). In response, three locations: A, B, and C, shown as Fig. 10, are selected as optimization targets. Similarly, the optimization strategies are proposed according to their characteristics and our research findings.

Location A, is covered by residential and industrial land and tends to present aggravated PM<sub>2.5</sub> with the increase of FAR. Combining the above urban ventilation map, appropriately reducing the plot ratio of the areas along the Yangtze River ventilation corridor is conducive to effective diffusion of pollutants into the water.

Location B, is developed in industrial land and surrounded by residential land. Overall, the FAR of residential land in Wuhan is higher than that of industrial land. Although high-rise residential buildings can effectively block the invasion of external PM<sub>2.5</sub> pollution, internal industrial pollution is not conducive to the diffusion of PM<sub>2.5</sub> concentration along the Han River. Mitigation strategies for location B should take action, such as relocating industrial land, reducing the density of surrounding residential zone along the Han River, and improving ventilation conditions.

Location C, is covered by residential land next to WISCO. The windward side of the building can resist the invasion of pollutants emitted by WISCO. As a response, appropriately increasing FAR of the land parcels adjacent to WISCO will hinder pollution. Meanwhile, it's necessary to allocate more green and open spaces, and properly demolish some heavily polluting enterprises.

## 6. Conclusion

This study innovatively introduces deep learning simulation

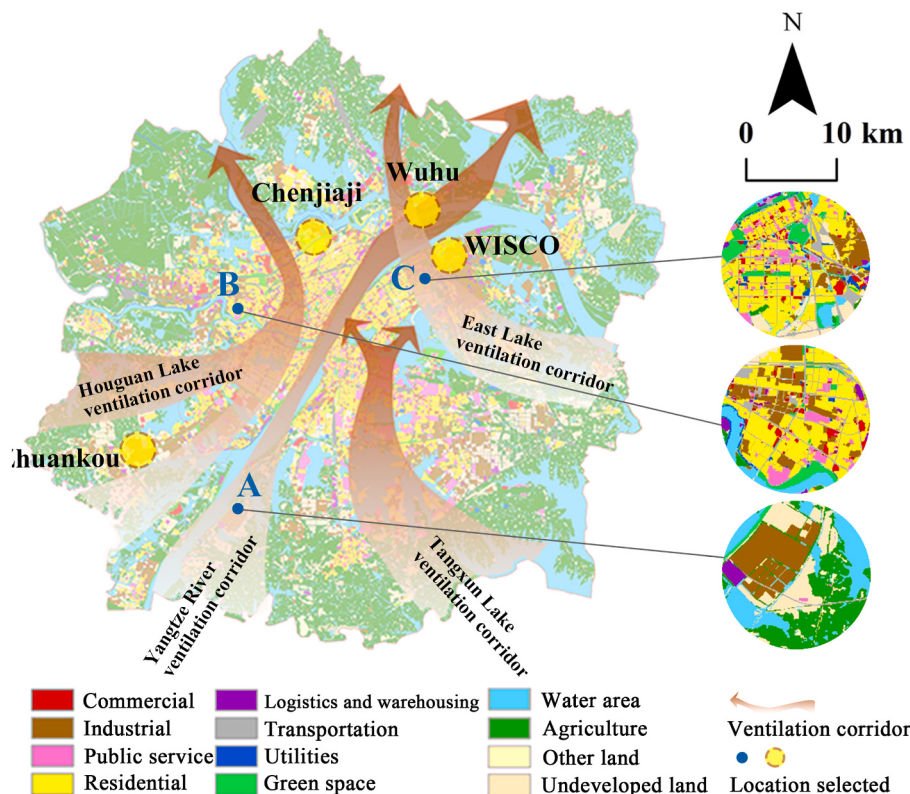


Fig. 10. Optimization strategies maps: Urban ventilation corridors and locations selected.

technology to explore the relationship among meteorological conditions, urban land use types, land use intensity and PM<sub>2.5</sub> concentration based on multi-source spatial data. By proposing deep learning simulation technology and setting different scenarios, the impact of urban land use types on PM<sub>2.5</sub> concentration distribution are quantified and spatially visualized. The results indicate that PM<sub>2.5</sub> pollution caused by industrial, residential, transportation, logistics and warehousing, commercial, utilities and public service land has decreased in sequence, while green space has a good dissipative effect on PM<sub>2.5</sub> pollution. There are spatial differences in the impact of increasing density on PM<sub>2.5</sub>, with most urban construction areas presenting alleviated pollution and a few locations experiencing heavier pollution. Based on the results of the impact analysis and the current situation of PM<sub>2.5</sub> pollution, the spatial optimization strategies to reduce PM<sub>2.5</sub> pollution are proposed. These theoretical research results can be applied to the urban planning spatial practices to reduce PM<sub>2.5</sub> pollution.

Incorporating meteorological conditions to investigate the influence of urban land use types on PM<sub>2.5</sub> pollution can provide a more scientific and reliable analysis. This study proposes a new deep learning simulation approach to investigate the correlation between land use and air pollution, and provides intuitive spatial adaptation strategies to alleviate pollution. It provides spatial technical support to simulate the relationship between land use and PM<sub>2.5</sub> from the perspective of integrated urban planning and artificial intelligence. Future improvements will focus on visualizing of the internal relationship behind the black box in the deep learning method. In addition, the Kriging interpolation map of PM<sub>2.5</sub> are not accurate as the actual data, although a large amount of point data from monitoring stations can achieve accurate estimation. In further study, better spatial data sources will provide more detailed information.

## CRediT authorship contribution statement

**Liyuan Zhao:** Writing – review & editing, Writing – original draft, Supervision, Methodology, Formal analysis, Conceptualization. **Ming Zhang:** Software, Methodology, Formal analysis, Conceptualization. **Si Cheng:** Methodology, Formal analysis, Data curation. **Yunhao Fang:** Visualization, Methodology. **Shuxian Wang:** Visualization, Data curation. **Cong Zhou:** Visualization.

## Declaration of competing interest

The authors declare that they have no known competing financial interests or personal relationships that could have appeared to influence the work reported in this paper.

## Data availability

Data will be made available on request.

## Acknowledgments

This work was supported by the National Natural Science Founding of China (72131008) and the Open Projects of Wuhan Research Institute (IWH20211011), and the Fundamental Research Funds for the Central Universities (2023WKZDJC009).

## References

- [1] N.N. Linh Thao, S. Pimonsree, K. Prueksakorn, P.T. Bich Thao, P. Vongruang, Public health and economic impact assessment of PM<sub>2.5</sub> from open biomass burning over countries in mainland Southeast Asia during the smog episode, *Atmos. Pollut. Res.* 13 (2022), 101418, <https://doi.org/10.1016/j.apr.2022.101418>.
- [2] D. Lu, J. Xu, W. Yue, W. Mao, D. Yang, J. Wang, Response of PM<sub>2.5</sub> pollution to land use in China, *J. Clean. Prod.* 244 (2020), 118741, <https://doi.org/10.1016/j.jclepro.2019.118741>.
- [3] S.H. Park, D.W. Ko, Investigating the effects of the built environment on PM<sub>2.5</sub> and PM10: a case study of Seoul Metropolitan city, South Korea, *Sustainability* 10 (12) (2018) 4552, <https://doi.org/10.3390/su10124552>.
- [4] C. Lee, How do built environments measured at two scales influence PM2.5 concentrations? *Transport Res D-Tr E* 99 (2021), 103014 <https://doi.org/10.1016/j.trd.2021.103014>.
- [5] S. Weichenthal, W. Farrell, M. Goldberg, L. Joseph, M. Hatzopoulou, Characterizing the impact of traffic and the built environment on near-road ultrafine particle and black carbon concentrations, *Environ. Res.* 132 (2014) 305–310, <https://doi.org/10.1016/j.envres.2014.04.007>.
- [6] L. Mao, Y. Qiu, C. Kusano, X. Xu, Predicting regional space-time variation of PM<sub>2.5</sub> with land-use regression model and MODIS data, *Environ. Sci. Pollut. Res.* 19 (2012) 128–138, <https://doi.org/10.1007/s11356-011-0546-9>.
- [7] R. Cervero, J. Murakami, Effects of built environments on vehicle miles traveled: evidence from 370 US urbanized areas, *Environ. Plann. A* 42 (2010) 400–418, <https://doi.org/10.1068/a4236>.
- [8] R. Ewing, R. Cervero, Travel and the built environment: a meta-analysis, *J. Am. Plann. Assoc.* 76 (2010) 265–294, <https://doi.org/10.1080/01944361003766766>.
- [9] M. Leroutier, P. Quirion, Air pollution and CO<sub>2</sub> from daily mobility: who emits and Why? Evidence from Paris, *Energy Econ.* 109 (2022), 105941, <https://doi.org/10.1016/j.eneco.2022.105941>.
- [10] J. Li, L. Wang, F. Zhao, Epigenetics-based individual interventions against the health risks of PM<sub>2.5</sub>, *Sci. Bull.* 62 (2017) 743–744, <https://doi.org/10.1016/j.scib.2017.05.009>.
- [11] X. Yang, Y. Zheng, G. Geng, H. Liu, H. Man, Z. Lv, K. He, K. de Hoogh, Development of PM<sub>2.5</sub> and NO<sub>2</sub> models in a LUR framework incorporating satellite remote sensing and air quality model data in Pearl River Delta region, China, *Environ. Pollut.* 226 (2017) 143–153, <https://doi.org/10.1016/j.envpol.2017.03.079>.
- [12] C.C. Chen, Y.R. Wang, H.Y. Yeh, T.H. Lin, C.S. Huang, C.F. Wu, Estimating monthly PM<sub>2.5</sub> concentrations from satellite remote sensing data, meteorological variables, and land use data using ensemble statistical modeling and a random forest approach, *Environ. Pollut.* 291 (2021), 118159, <https://doi.org/10.1016/j.envpol.2021.118159>.
- [13] P.Y. Wong, H.Y. Lee, Y.C. Chen, Y.T. Zeng, Y.R. Chern, N.T. Chen, S.C. Candice Lung, H.J. Su, C.D. Wu, Using a land use regression model with machine learning to estimate ground level PM<sub>2.5</sub>, *Environ. Pollut.* 277 (2021), 116846, <https://doi.org/10.1016/j.envpol.2021.116846>.
- [14] W.J. Requia, B.A. Coull, P. Kourtrakis, Evaluation of predictive capabilities of ordinary geostatistical interpolation, hybrid interpolation, and machine learning methods for estimating PM<sub>2.5</sub> constituents over space, *Environ. Res.* 175 (2019) 421–433, <https://doi.org/10.1016/j.envres.2019.05.025>.
- [15] C. Lee, Impacts of multi-scale urban form on PM<sub>2.5</sub> concentrations using continuous surface estimates with high-resolution in U.S. metropolitan areas, *Landsat Urban Plann.* 204 (2020), 103935, <https://doi.org/10.1016/j.landurbplan.2020.103935>.
- [16] C. Sun, W. Zhang, Y. Luo, Y. Xu, The improvement and substitution effect of transportation infrastructure on air quality: an empirical evidence from China's rail transit construction, *Energy Pol.* 129 (2019) 949–957, <https://doi.org/10.1016/j.enpol.2019.03.005>.
- [17] L. Zhao, T. Li, A. Przybysz, Y. Guan, P. Ji, B. Ren, C. Zhu, Effect of urban lake wetlands and neighboring urban greenery on air PM10 and PM<sub>2.5</sub> mitigation, *Build. Environ.* 206 (2021), 108291, <https://doi.org/10.1016/j.buildenv.2021.108291>.
- [18] X. Liu, C. Guo, Y. Wu, C. Huang, K. Lu, Y. Zhang, L. Duan, M. Cheng, F. Chai, F. Mei, H. Dai, Evaluating cost and benefit of air pollution control policies in China: a systematic review, *J. Environ. Sci.* 123 (2023) 140–155, <https://doi.org/10.1016/j.jes.2022.02.043>.
- [19] K. Yang, Y. Shi, Y. Luo, R. Liu, W. Sun, M. Sun, Assessing spatiotemporal air environment degradation and improvement represented by PM<sub>2.5</sub> in China using two-phase hybrid model, *Sustain. Cities Soc.* 59 (2020), 102180, <https://doi.org/10.1016/j.scs.2020.102180>.
- [20] Q. Guo, D. Wu, C. Yu, T. Wang, M. Ji, X. Wang, Impacts of meteorological parameters on the occurrence of air pollution episodes in the Sichuan basin, *J. Environ. Sci.* 114 (2022) 308–321, <https://doi.org/10.1016/j.jes.2021.09.006>.
- [21] S. Duan, Q. Liu, D. Jiang, Y. Jiang, Y. Lin, Z. Gong, Exploring the joint impacts of natural and built environments on PM<sub>2.5</sub> concentrations and their spatial heterogeneity in the context of high-density Chinese cities, *Sustainability* 13 (2021), 11775, <https://doi.org/10.3390/su132111775>.
- [22] Z. Chen, X. Xie, J. Cai, D. Chen, B. Gao, B. He, N. Cheng, B. Xu, Understanding meteorological influences on PM<sub>2.5</sub> concentrations across China: a temporal and spatial perspective, *Atmos. Chem. Phys.* 18 (8) (2018) 5343–5358, <https://doi.org/10.5194/acp-18-5343-2018>.
- [23] Z. Zou, C. Cheng, S. Shen, The complex nonlinear coupling causal patterns between PM<sub>2.5</sub> and meteorological factors in Tibetan Plateau: a Case Study in Xining, *IEEE Access* 9 (2021): 150373–150382, doi:10.1109/ACCESS.2021.3123455.
- [24] X. Li, C. Wu, M.E. Meadows, Z. Zhang, X. Lin, Z. Zhang, Y. Chi, M. Feng, E. Li, Y. Hu, Factors underlying spatiotemporal variations in atmospheric PM<sub>2.5</sub> concentrations in Zhejiang Province, China, *Remote Sens-Basel* 13 (2021) 3011, <https://doi.org/10.3390/rs13153011>.
- [25] X. Sun, X.S. Luo, J. Xu, Z. Zhao, Y. Chen, L. Wu, Q. Chen, D. Zhang, Spatio-temporal variations and factors of a provincial PM<sub>2.5</sub> pollution in eastern China during 2013–2017 by geostatistics, *Sci. Rep.* 9 (2019) 3613, <https://doi.org/10.1038/s41598-019-40426-8>.
- [26] L. Liu, X. Wan, G. Yang, Comment on “mortality effects assessment of ambient PM<sub>2.5</sub> pollution in the 74 leading cities of China” by die fang, qin'geng wang,

- huiming Li, yiyong yu, yan Lu, xin qian, Sci. Total Environ. 618 (15) (2018) 595–596, <https://doi.org/10.1016/j.scitotenv.2017.03.257>.
- [27] J. Yuan, Y. Wu, W. Jing, J. Liu, M. Du, Y. Wang, M. Liu, Association between meteorological factors and daily new cases of COVID-19 in 188 countries: a time series analysis, Sci. Total Environ. 780 (2021), 146538, <https://doi.org/10.1016/j.scitotenv.2021.146538>.
- [28] K.R. Baker, K.M. Foley, A nonlinear regression model estimating single source concentrations of primary and secondarily formed PM<sub>2.5</sub>, Atmos. Environ. 45 (2011) 3758–3767, <https://doi.org/10.1016/j.atmosenv.2011.03.074>.
- [29] K. Dimitriou, P. Kassomenos, A study on the reconstitution of daily PM<sub>10</sub> and PM<sub>2.5</sub> levels in Paris with multivariate linear regression model, Atmos. Environ. 98 (2014) 648–654, <https://doi.org/10.1016/j.atmosenv.2014.09.047>.
- [30] Z. He, P. Liu, X. Zhao, X. He, J. Liu, Y. Mu, Responses of surface O<sub>3</sub> and PM<sub>2.5</sub> trends to changes of anthropogenic emissions in summer over Beijing during 2014–2019: a study based on multiple linear regression and WRF-Chem, Sci. Total Environ. 807 (2022), 150792, <https://doi.org/10.1016/j.scitotenv.2021.150792>.
- [31] B. Zou, Z. Zheng, N. Wan, Y. Qiu, J.G. Wilson, An optimized spatial proximity model for fine particulate matter air pollution exposure assessment in areas of sparse monitoring, Int. J. Geogr. Inf. Sci. 30 (2016) 727–747, <https://doi.org/10.1080/13658816.2015.1095921>.
- [32] P. Zhang, W. Ma, F. Wen, L. Liu, L. Yang, J. Song, N. Wang, Q. Liu, Estimating PM<sub>2.5</sub> concentration using the machine learning GA-SVM method to improve the land use regression model in Shaanxi, China, Ecotoxicol. Environ. Saf. 225 (2021), 112772, <https://doi.org/10.1016/j.ecoenv.2021.112772>.
- [33] J. Luo, P. Du, A. Samat, J. Xia, M. Che, Z. Xue, Spatiotemporal pattern of PM<sub>2.5</sub> concentrations in mainland China and analysis of its influencing factors using geographically weighted regression, Sci. Rep. 7 (2017), 40607, <https://doi.org/10.1038/srep40607>.
- [34] S. Zhou, R. Lin, Spatial-temporal heterogeneity of air pollution: the relationship between built environment and on-road PM<sub>2.5</sub> at micro scale, Transport Res D-Tr E 76 (2019) 305–322, <https://doi.org/10.1016/j.trd.2019.09.004>.
- [35] Z. Chen, D. Chen, C. Zhao, M. Kwan, J. Cai, Y. Zhuang, B. Zhao, X. Wang, B. Chen, J. Yang, R. Li, B. He, B. Gao, K. Wang, B. Xu, Influence of meteorological conditions on PM<sub>2.5</sub> concentrations across China: a review of methodology and mechanism, Environ. Int. 139 (2020), 105558, <https://doi.org/10.1016/j.envint.2020.105558>.
- [36] Y. Fan, J. Hunt, Q. Wang, Y. Li, Inversion breakup over different shapes of urban areas, Build. Environ. 190 (2021), 107548, <https://doi.org/10.1016/j.buildenv.2020.107548>.
- [37] M.A. Khan, S. Kwon, J. Choo, S.M. Hong, S.H. Kang, I.H. Park, S.K. Kim, S.J. Hong, Automatic detection of tympanic membrane and middle ear infection from otoscopic images via convolutional neural networks, Neural Network. 126 (2020) 384–394, <https://doi.org/10.1016/j.neunet.2020.03.023>.
- [38] V.T. Pham, T.T. Tran, P.C. Wang, P.Y. Chen, M.T. Lo, EAR-UNet: a deep learning-based approach for segmentation of tympanic membranes from otoscopic images, Artif. Intell. Med. 115 (2021), 102065, <https://doi.org/10.1016/j.artmed.2021.102065>.
- [39] H. Zunair, A. Ben Hamza, Sharp U-Net, Depthwise convolutional network for biomedical image segmentation, Comput. Biol. Med. 136 (2021), 104699, <https://doi.org/10.1016/j.combiomed.2021.104699>.
- [40] L. Parisi, D. Neagu, R. Ma, F. Campean, Quantum ReLU activation for convolutional neural networks to improve diagnosis of Parkinson's disease and COVID-19, Expert Syst. Appl. 187 (2022), 115892, <https://doi.org/10.1016/j.eswa.2021.115892>.
- [41] M. Toğuçar, B. Ergen, Classification of cloud images by using super resolution, semantic segmentation approaches and binary sailfish optimization method with deep learning model, Comput. Electron. Agric. 193 (2022), 106724, <https://doi.org/10.1016/j.compag.2022.106724>.
- [42] W. Chen, A.N. Wu, F. Biljecki, Classification of urban morphology with deep learning: application on urban vitality, Comput. Environ. Urban 90 (2021), 101706, <https://doi.org/10.1016/j.compenvurbsys.2021.101706>.
- [43] Y. Fan, X. Ding, J. Wu, J. Ge, Y. Li, High spatial-resolution classification of urban surfaces using a deep learning method, Build. Environ. 200 (2021), 107949, <https://doi.org/10.1016/j.buildenv.2021.107949>.
- [44] Y. Zhang, S. Li, R. Dong, H. Deng, X. Fu, C. Wang, T. Yu, T. Jia, J. Zhao, Quantifying physical and psychological perceptions of urban scenes using deep learning, Land Use Pol. 111 (2021), 105762, <https://doi.org/10.1016/j.landusepol.2021.105762>.
- [45] J. Jagannathan, C. Divya, Deep learning for the prediction and classification of land use and land cover changes using deep convolutional neural network, Ecol. Inf. 65 (2021), 101412, <https://doi.org/10.1016/j.ecoinf.2021.101412>.
- [46] Q. Cai, M. Abdel-Aty, Y. Sun, J. Lee, J. Yuan, Applying a deep learning approach for transportation safety planning by using high-resolution transportation and land use data, Transport Res A-Pol 127 (2019) 71–85, <https://doi.org/10.1016/j.tra.2019.07.010>.
- [47] T. Zhao, Z. Huang, W. Tu, B. He, R. Cao, J. Cao, M. Li, Coupling graph deep learning and spatial-temporal influence of built environment for short-term bus travel demand prediction, Comput. Environ. Urban 94 (2022), 101776, <https://doi.org/10.1016/j.compenvurbsys.2022.101776>.
- [48] N. Ahmed, M.N. Islam, A.S. Tuba, M.R.C. Mahdy, M. Sujauddin, Solving visual pollution with deep learning: a new nexus in environmental management, J. Environ. Manag. 248 (2019), 109253, <https://doi.org/10.1016/j.jenvman.2019.07.024>.
- [49] K.K.R. Samal, K.S. Babu, S.K. Das, Multi-directional temporal convolutional artificial neural network for PM<sub>2.5</sub> forecasting with missing values: a deep learning approach, Urban Clim. 36 (2021), 100800, <https://doi.org/10.1016/j.ulclim.2021.100800>.
- [50] S.C. Koumetio Tekouabou, E.B. Diop, R. Azmi, R. Jaligot, J. Chenal, Reviewing the application of machine learning methods to model urban form indicators in planning decision support systems: potential, issues and challenges, J King Saud Univ-Com 34 (2022) 5943–5967, <https://doi.org/10.1016/j.jksuci.2021.08.007>.
- [51] J. Zhao, W. Fan, X. Zhai, Identification of land-use characteristics using bicycle sharing data: a deep learning approach, J. Transport Geogr. 82 (2020), 102562, <https://doi.org/10.1016/j.jtrangeo.2019.102562>.
- [52] Z. Xu, L. Niu, Z. Zhang, Q. Hu, D. Zhang, J. Huang, C. Li, The impacts of land supply on PM<sub>2.5</sub> concentration: evidence from 292 cities in China from 2009 to 2017, J. Clean. Prod. 347 (2022), 131251, <https://doi.org/10.1016/j.jclepro.2022.131251>.
- [53] X. Chen, X. Wang, X. Wu, J. Guo, Z. Zhou, Influence of roadside vegetation barriers on air quality inside urban street canyons, Urban For Urban Gree 63 (2021), 127219, <https://doi.org/10.1016/j.ufug.2021.127219>.
- [54] X. Wang, M. Teng, C. Huang, Z. Zhou, X. Chen, Y. Xiang, Canopy density effects on particulate matter attenuation coefficients in street canyons during summer in the Wuhan metropolitan area, Atmos. Environ. 240 (2020), 117739, <https://doi.org/10.1016/j.atmosenv.2020.117739>.
- [55] F. Ikemori, K. Uraishi, D. Asakawa, R. Nakatsubo, M. Makino, M. Kido, N. Mitamura, K. Asano, S. Nonaka, R. Nishimura, S. Sugata, Source apportionment in PM<sub>2.5</sub> in central Japan using positive matrix factorization focusing on small-scale local biomass burning, Atmos. Pollut. Res. 12 (2021) 162–172, <https://doi.org/10.1016/j.apr.2021.01.006>.
- [56] L. Zhao, C. Liu, X. Liu, K. Liu, Y. Shi, Urban spatial structural options for air pollution control in China: evidence from provincial and municipal levels, Energy Rep. 7 (2021) 93–105, <https://doi.org/10.1016/j.egyr.2021.10.050>.
- [57] F. Boukouvala, F.J. Muzzio, M.G. Ierapetritou, Dynamic data-driven modeling of Pharmaceutical processes, Ind. Eng. Chem. Res. 50 (2011) 6743–6754, <https://doi.org/10.1021/ie102305a>.
- [58] H. Zhang, Y. Zhan, J. Li, C.Y. Chao, Q. Liu, C. Wang, S. Jia, L. Ma, P. Biswas, Using Kriging incorporated with wind direction to investigate ground-level PM<sub>2.5</sub> concentration, Sci. Total Environ. 751 (2021), 141813, <https://doi.org/10.1016/j.scitotenv.2020.141813>.
- [59] S. Kutluk, K. Kayabol, A. Akan, A new CNN training approach with application to hyperspectral image classification, Digit. Signal Process. 113 (2021), 103016, <https://doi.org/10.1016/j.dsp.2021.103016>.
- [60] G. Zhao, G. Liu, L. Fang, B. Tu, P. Ghamsari, Multiple convolutional layers fusion framework for hyperspectral image classification, Neurocomputing 339 (2019) 149–160, <https://doi.org/10.1016/j.neucom.2019.02.019>.
- [61] H.N. Mhaskar, T. Poggio, Deep vs. shallow networks: an approximation theory perspective, Anal. Appl. 14 (6) (2016) 829–848, <https://doi.org/10.1142/S0219530516400042>.
- [62] S. Zubair, F. Yan, W. Wang, Dictionary learning based sparse coefficients for audio classification with max and average pooling, Digit. Signal Process. 23 (3) (2013) 960–970, <https://doi.org/10.1016/j.dsp.2013.01.004>.
- [63] A.P. Piotrowski, J.J. Napiorkowski, A.E. Piotrowska, Impact of deep learning-based dropout on shallow neural networks applied to stream temperature modelling, Earth Sci. Rev. 201 (2020), 103076, <https://doi.org/10.1016/j.earscirev.2019.103076>.
- [64] N.A. Zaini, L.W. Ean, A.N. Ahmed, M. Abdul Malek, M.F. Chow, PM<sub>2.5</sub> forecasting for an urban area based on deep learning and decomposition method, Sci. Rep. 12 (1) (2022), 17565.
- [65] J. Cohen, A coefficient of agreement for nominal scales, Educ. Psychol. Meas. 20 (1960) 37–46, <https://doi.org/10.1177/00131644600200104>.
- [66] X. Li, Q. Yang, X. Liu, Discovering and evaluating urban signatures for simulating compact development using cellular automata, Landsc. Urban Plann. 86 (2008) 177–186, <https://doi.org/10.1016/j.landurbplan.2008.02.005>.
- [67] L. Zhao, F. Liu, Land-use planning adaptation in response to SLR based on a vulnerability analysis, Ocean Coast Manag. 196 (2020), 105297, <https://doi.org/10.1016/j.ocecoaman.2020.105297>.
- [68] J.L. Fleiss, J. Cohen, B.S. Everitt, Large sample standard errors of kappa and weighted kappa, Psychol. Bull. 72 (5) (1969) 323–327, <https://doi.org/10.1037/h0028106>.
- [69] J.R. Landis, G.G. Koch, The measurement of observer agreement for categorical data, Biometrics 33 (1) (1977) 159–174.
- [70] Y. Xia, Chapter Eleven-Correlation and association analyses in microbiome study integrating multiomics in health and disease, Prog. Nucleic Acid Res. Mol. Biol. 171 (2020) 309–491, <https://doi.org/10.1016/bs.pmbts.2020.04.003>.
- [71] M. Chen, J. Bai, S. Zhu, B. Yang, F. Dai, The influence of neighborhood-level urban morphology on PM<sub>2.5</sub> variation based on random forest regression, Atmos. Pollut. Res. 12 (2021), 101147, <https://doi.org/10.1016/j.apr.2021.101147>.
- [72] S. Jung, S. Yoon, Analysis of the effects of floor area ratio change in urban street canyons on microclimate and particulate matter, Energies 14 (2021) 714, <https://doi.org/10.3390/en14030714>.
- [73] H. Xu, Y. Chen, Impact of urban morphology on the spatial and temporal distribution of PM<sub>2.5</sub> concentration: a numerical simulation with WRF/CMAQ model in Wuhan, China, J. Environ. Manag. 290 (2021), 112427, <https://doi.org/10.1016/j.jenvman.2021.112427>.
- [74] M. Yuan, Y. Song, Y. Huang, H. Shen, T. Li, Exploring the association between the built environment and remotely sensed PM<sub>2.5</sub> concentrations in urban areas, J. Clean. Prod. 220 (2019) 1014–1023, <https://doi.org/10.1016/j.jclepro.2019.02.236>.
- [75] T. Chen, M. Li, L. Luo, S. Deng, R. Zhou, D. Chen, Simulating the effects of land urbanization on regional meteorology and air quality in Yangtze River Delta, China, Appl. Geogr. 120 (2020), 102228, <https://doi.org/10.1016/j.apgeog.2020.102228>.